Marc T. Aronhime
Casali Institute of Applied Chemistry, The Hebrew University of Jerusalem, 91904 Jerusalem, Israel

John K. Gillham
Polymer Materials Program, Department of Chemical Engineering, Princeton University, Princeton, New Jersey 08544, USA

An isothermal time-temperature-transformation (TTT) cure diagram for thermosetting systems has been developed to aid in the understanding of the cure process and the properties after cure. The diagram summarizes in a convenient manner the temperature of cure (T_{cure}) vs. the times to gelation, vitrification, phase separation (in the case of rubber-modified systems), full cure, and thermal degradation. A more complete diagram could also include contours of constant conversion, viscosity, and modulus. The principal experimental technique which has been used to obtain a TTT diagram, torsional braid analysis (TBA), is described. Two recent models describing the cure process are revieved; from these the time to vitrification vs. T_{cure} is computed from the chemical kinetics and the conversion at vitrification. One model uses a relationship between T_g and the extent of conversion at vitrification in conjunction with experimental data for the extent of conversion at vitrification, whereas the other predicts the extent of conversion at T_g from relationships in the literature. Both models predict an S-shaped time to vitrification curve, as has been obtained experimentally. The second model has been applied also to linearly polymerizing systems.

Advances in Polymer Science 78

1 Introduction

The transformation of low molecular weight liquid into high molecular weight amorphous solid polymer by chemical reaction is the fundamental process used in the coatings, adhesives and thermoset industries. As the chemical reaction proceeds, the molecular weight and glass transition temperature (T_g) increase, and if the reaction is carried out isothermally below the glass transition temperature of the fully reacted system ($T_{g\infty}$), the polymer T_g will eventually reach the reaction temperature (T_{cure}). During isothermal reaction below $T_{g\infty}$, two phenomena of critical importance in thermosetting processing can occur: gelation and vitrification. For linear systems, only vitrification will occur. Gelation generally occurs first, and is characterized by the incipient formation of material of infinite molecular weight. Prior to gelation, the system is soluble and fusible, but after gelation both soluble (sol fraction) and insoluble (gel fraction) materials are present. As the reaction proceeds beyond gelation, the amount of gel increases at the expense of the sol. As gelation is approached, the viscosity increases dramatically, and the weight average molecular weight goes to infinity, but the number average molecular weight is small. Vitrification is the transformation from liquid or rubbery material to glassy material. At vitrification, the material solidifies and the chemical reactions can be quenched; T_g can therefore equal or exceed T_{cure}. Other parameters of importance in the thermosetting process include the changes in viscosity and conversion with time, and thermal degradation at high temperatures.

An isothermal time-temperature-transformation (TTT) cure diagram results if, for a series of isothermal cures, the temperature of cure (T_{cure}) is plotted vs. the times to gelation and vitrification [1–4]. The TTT diagram provides a framework for understanding the cure process of thermosetting (and linearly polymerizing) materials. Relationships between cure, structure and properties can also be understood by studying the TTT diagram. The TTT diagram can be extended to include phase separation (in the case of rubber-modified thermosets, for example), viscosity, thermal degradation, and extent of conversion.

Much of the behavior of thermosetting materials can be clarified in terms of the TTT cure diagram through the influence of gelation, vitrification and devitrification on properties. For example, gelation retards macroscopic flow, and limits the growth of a dispersed phase (as in rubber-modified systems); vitrification retards chemical conversion; and devitrification, due to thermal degradation marks, the limit in time for the material to support a substantial load.

The TTT diagram is a familiar concept in materials science for studying phase changes [5]. The TTT diagram is a nonequilibrium diagram, since the transformations occur as functions of time. TTT diagrams have played an important role in the control of the properties of metals by permitting thermal history paths to be chosen so that a desired microstructure can be obtained. The diagrams are specific to a particular material composition and considerable insight into the design of alloys can be achieved once the effects of additives on the TTT diagram have been explored. Such a diagram for thermosetting systems would permit time-temperature paths of cure to be chosen so that gelation, vitrification, and phase separation occur in a controlled manner and consequently give rise to predictable properties of the thermosetting matrix [2].

The purpose of this review is to summarize the basic features and utility of the TTT cure diagram, discuss the experimental procedures for obtaining a diagram, present experimentally-obtained diagrams for model systems, and describe recent models that have attempted to calculate the time to vitrification on isothermal polymerization. This review will concentrate on TTT diagrams of epoxy systems.

2 Generalized Schematic TTT Cure Diagram

A schematic TTT cure diagram, illustrating the main features of the thermosetting process, is shown in Fig. 1. The diagram indicates distinct regions of matter encountered in the thermosetting process; these include liquid, sol/gel rubber, gel rubber, sol/gel glass, gel glass, sol glass, and char. Three critical temperatures are also shown: T_{go}, ${}_{gel}T_g$, and $T_{g\infty}$. A "full cure" line is indicated on the diagram which separates the sol/gel rubber region from the gel rubber region, and the sol/gel glass region from the gel glass region. Isoviscosity contours, the onset of phase separation, and thermal degradation events are also included. Finally, note that the temperature of cure vs. the time to vitrification curve is S shaped.

T_{go} is the glass transition temperature of the uncured reactants. Below this temperature, in principle the system has no reactivity. ${}_{gel}T_g$ is the temperature at which gelation and vitrification coincide. Between T_{go} and ${}_{gel}T_g$ the system will vitrify before

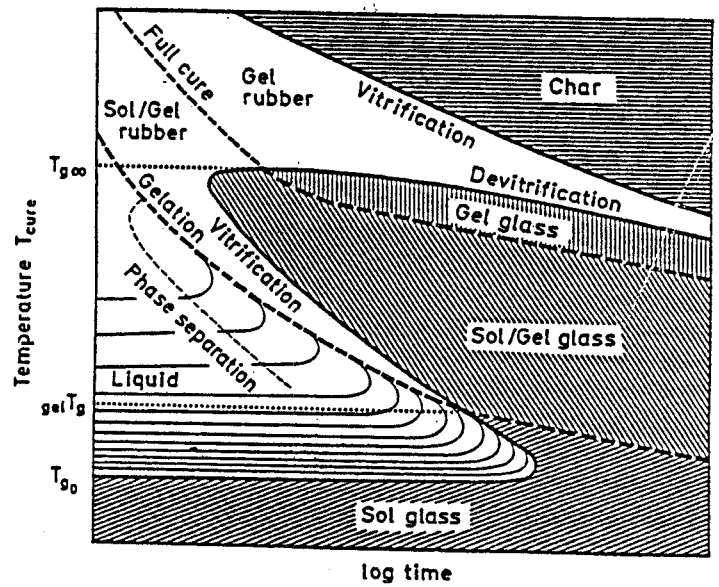

Fig. 1. Schematic time-temperature-transformation (TTT) isothermal cure diagram for a thermosetting system, showing three critical temperatures (T_{go}, ${}_{gel}T_g$, $T_{g\infty}$) and distinct regions of matter (liquid, sol/gel rubber, gel rubber, sol/gel glass, gel glass, sol glass, char). The full cure line ($T_g = T_{g\infty}$) separates the sol/gel glass from the gel glass region, and the sol/gel rubber from the gel elastomer region, respectively. Degradation events are devitrification and char formation. The successive isoviscous contours shown in the liquid region, which were calculated in the absence of phase separation, differ by a factor of ten. Phase separation occurs in the liquid region prior to gelation

gelling, in principle quenching the chemical reactions, and thus precluding gelation. At vitrification below ${}_{gel}T_g$, the system is of low molecular weight, and on subsequent heating the material will flow and is readily processable.

$T_{g\infty}$ is the maximum glass transition temperature of the system. Between ${}_{gel}T_g$ and $T_{g\infty}$, the material is initially in the liquid region, and is soluble and of low molecular weight. On reaction, gelation occurs, and the sol/gel rubber region is entered. Finite molecular weight sol and infinite molecular weight gel generally form a miscible binary mixture in this region. Eventually, T_g will rise to T_{cure}, and vitrification will be said to occur. Vitrification greatly decreases the molecular and submolecular mobilities, and thus in principle the chemical reactions are quenched. In the absence of full cure, the vitrified region formed between ${}_{gel}T_g$ and $T_{g\infty}$ contains both sol and gel components.

However, recent work investigating the cure behavior after vitrification has shown that reactions do occur in the glassy state on prolonged isothermal cure beyond vitrification [4]. The "full cure" line in Fig. 1 is the time required, for any given T_{cure}, for T_g to equal $T_{g\infty}$. Thus, the glass region between ${}_{gel}T_g$ and $T_{g\infty}$ is subdivided into two regions: 1) the sol/gel glass region, below the full cure line where the cure is not yet complete; and 2) the gel glass region, above the full cure line where in principle the system is fully reacted as determined by T_g measurements.

The determination of full cure is important because meaningful structure-property relationships between different systems can only be made by considering fully cured materials. If the cure state of a material is unknown, then its properties can not be compared with those of another material, whose cure state is also unknown, for the purpose of relating the observed properties to the chemical structures. For systems where $T_{g\infty}$ can be attained in the absence of degradation, curing above $T_{g\infty}$ is the most direct method for achieving full cure. For high temperature systems, where curing above $T_{g\infty}$ would lead to thermal degradation, the full cure line (Fig. 1) presents an alternative guide for achieving complete cure; the system can be cured below $T_{g\infty}$, thus avoiding degradation.

In a manner similar to the extension of the full cure line into the glassy region, note that the gelation line is extended beyond the vitrification curve (Fig. 1). This implies that gelation can occur below ${}_{gel}T_g$ once vitrification has occurred; this could affect the storage temperature of partially-reacted materials.

On isothermal reaction above $T_{g\infty}$, the material will gel but not vitrify in the absence of degradation. An elastomer (gel rubber) is formed above $T_{g\infty}$ after prolonged isothermal cure, as indicated by the full cure line.

The calculation of the S-shaped time to vitrification curve forms the basis of Section 4 of this review. The local maximum just above T_{g0} and the local minimum just below $T_{g\infty}$ arise from kinetic factors. The minimum in the time to vitrification is important in molding applications when the mold can not be opened until the system has solidified. However, as is discussed later, the time to vitrification curve need not be S-shaped, but can assume a sigmoidal shape, depending upon the values of the kinetic parameters used in the model.

The isoviscosity contours of Fig. 1 increase by one order of magnitude from one curve to the one below it. At high temperature the initial viscosity is naturally lower than the viscosity at low temperature, but the viscosity increases much more rapidly

at high than at low temperatures. The fluid state is limited by gelation above ${}_{gel}T_g$ and by vitrification between T_g and ${}_{gel}T_g$ [6]. By visual extrapolation of the isoviscosity curves, the vitrification curve below ${}_{gel}T_g$ appears to be an isoviscous contour: this is a consequence of the method of computing the isoviscosity curves [6]. The change in viscosity with time is one of the most important parameters in thermoset processing. An isoviscosity level is often used as a practical measure of gelation. In the glassy state, the isomodulus contours would be expected to approximately parallel the vitrification curve.

Isoconversion curves, if shown, would approximately parallel the gelation line (as well as the full cure line) because gelation is considered to be an isoconversion state [7]. The extent of conversion after vitrification changes very slowly, but does not cease. Reference to a complete TTT diagram enables a time-temperature path of cure to be selected which will follow a desired viscosity-conversion path.

In the case of a rubber-modified thermoset, the cloud point marks the visual onset of phase separation of the rubber-rich domains from an initially homogeneous solution of reactants. The cloud point can be observed by a dramatic decrease in the intensity of transmitted light, or a dramatic increase in the intensity of scattered light. Whereas most of the phase separation will occur prior to gelation, the end of phase separation can occur after gelation [8]. Phase separation is influenced by competing thermodynamic and kinetic (transport) factors. At low temperatures, nucleation of a dispersed phase is favored thermodynamically but transport to nucleating sites is reduced due to the high viscosities and low temperatures. At high temperatures, the nucleation rate is low, but the low viscosity and high temperatures facilitate the transport. Thus a maximum in the amount of precipitated rubber is anticipated at an intermediate temperature which could give rise to a minimum in the T_{cure} vs. time to phase separation curve [2].

At high temperatures thermal degradation becomes important, and may prevent full cure from being achieved [3]. Two degradation events have been noted in relation to the TTT diagram: devitrification followed by elastomer formation; and vitrification followed by char formation. The devitrification event corresponds to a decrease in T_g from above to below the isothermal cure temperature; the time to this event may be considered to be the lifetime of the material since it marks the limit in time for the material to support a substantial load. The second event is an elastomer-to-glass transformation, accompanied by an increase in T_g and rigidity, and is presumably due to the onset of char formation [3].

The TTT diagram (Fig. 1) is a convenient tool for summarizing the changes in material parameters that occur during the thermosetting process. The necessary time-temperature paths of cure to achieve desired viscosity-conversion levels, the onset and end of phase separation, and the proper cure paths to avoid thermal degradation can be gleaned from examination of a complete TTT cure diagram.

3 Experimental Aspects of the TTT Cure Diagram

3.1 Torsional Braid Analysis (TBA)

The isothermal TTT cure diagram summarizes the transitions that occur on isothermal polymerization, such as gelation, vitrification and devitrification. Typically,

the cure process is followed from the initial liquid state, through gelation and the sol/gel rubber region, and into the vitrified region. The cured material is then subjected to a dynamic temperature scan at a fixed scanning rate in order to determine the T_g and other transition temperatures after cure.

A convenient method for determining transition times and transition temperatures of polymeric materials is dynamic mechanical analysis. One type of instrument which is particularly suitable for polymeric solids is the freely oscillating torsion pendulum (TP). Advantages of the TP include its simplicity, sensitivity, relatively low frequency (~1 Hz) which permits direct correlation of transition temperatures with static non-mechanical methods (e.g., dilatometry and calorimetry), and its high resolution of transitions [2]. A major disadvantage of the conventional TP is that test temperatures are limited by the inability of materials to support their own weight near load-limiting transition temperatures.

A variation of the TP is torsional braid analysis (TBA) [2,9], in which a small sample of the material is supported on a multifilamented glass braid. The TBA technique has the distinct advantage of being able to take measurements throughout the cure process, since properties can be recorded above the load-limiting temperatures of the reactants. Monitoring the entire cure process is essential if a TTT cure diagram is to be constructed. The elastic and loss moduli of the composite specimen (resin plus glass substrate) are calculated from the damped oscillations of each wave and changes are interpreted in terms of the properties of the supported material.

A schematic diagram of the torsion pendulum is shown in Fig. 2. The pendulum is intermittently set into motion to generate a series of damped oscillations while the material behavior of the specimen changes with temperature and/or time. The time scale of the change in the material is much greater than the time scale of one damped wave. The nondriven, free oscillations are initiated by an angular step-displacement of the fixed end of the specimen. The natural frequency range of the vibrations is 0.05–5 Hz. Conversion of the damped oscillations to electrical analogue signals is accomplished using a transducer.

A key factor in the instrumentation was the development of a nondrag, optical transducer that produces an electrical response that is a linear function of the angular deformation of the pendulum. A polarizing disk is employed as the inertial member of the pendulum, and a stationary second polarizer is positioned in front of a photodetector whose response is a linear function of intensity. The intensity of light transmission through two polarizers is a cosine squared function of their angular displacement; over a useful range symmetrical between the crossed and parallel positions of the pair of polarizers, the transmission function approaches linearity. As the properties of the specimen change, twisting of the specimen may cause the inertial mass polarizer to drift out of the linear range. An automated control sequence was designed to compensate for this behavior [2].

The composite specimen is supported in the cylindrical vertical shaft in a copper block around which are band heaters, and cooling coils for liquid nitrogen. The instrument generally operates over a temperature range of −190 to 400 °C with a temperature spread of <1 °C over a two inch specimen. (The instrument has been modified to give greater temperature ranges [2].) A temperature programmer/controller permits isothermal, linearly increasing and linearly decreasing temperature

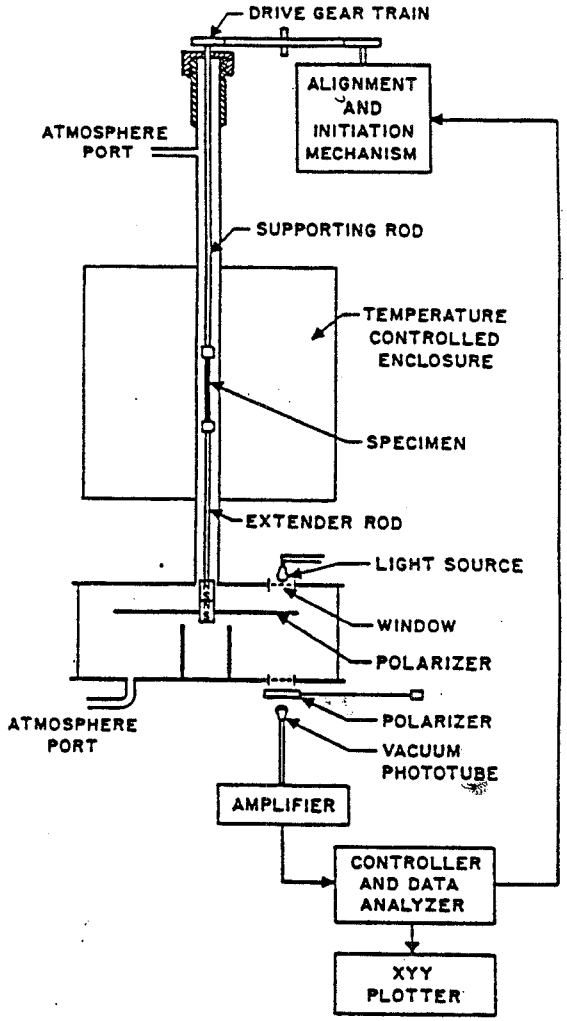

Fig. 2. Automated torsion pendulum: schematic. An analog electrical signal results from using a light beam passing through a pair of polarizers, one of which oscillates with the pendulum. The pendulum is aligned for linear response and initiated by a computer that also processes the damped waves to provide the elastic modulus and mechanical damping data, which are plotted vs. temperature or time

modes of operation to be made. The atmosphere is tightly controlled, and for cure studies an inert atmosphere is generally desired; dry helium is used, rather than nitrogen, because helium has better heat transfer properties at low temperatures.

The substrate used is a heat-cleaned (425 °C/3 h in air) glass braid, two inches long, containing about 3600 filaments. A braid is used because it has a balanced twist. The large surface area of the braid permits pickup of relatively large amounts of fluid and minimizes flow due to gravity. In most TBA experiments, the reactants are dissolved in a suitable solvent [generally methylethyl ketone (MEK) for epoxy systems] in the ratio of 1 g solids/1 ml solvent. The solvent is removed from the solution-impregnated braid in situ by heating the composite specimen above the boiling point of the solvent.

The TBA/TP instrumental system is available from Plastics Analysis Instruments, Inc., Princeton, New Jersey, USA.

3.2 Relationship of TBA Parameters to Material Parameters

Two mechanical functions of the specimen, rigidity and damping, are obtained from the frequency and decay constants which characterize each wave. TBA experiments provide plots of relative rigidity ($1/P^2$, where P is the period of the oscillation) and logarithmic decrement ($\Delta = \ln [\theta_i/\theta_{i+1}]$, where θ_i is the amplitude of the ith oscillation of the freely damped wave) vs. either time or temperature. The relative rigidity is proportional to G′, the elastic shear modulus; the logarithmic decrement is proportional to G″/G′, where G″ is the out-of-phase shear modulus. Due to the composite nature of the TBA specimen, quantitative values of G′ and G″ are not obtained. However, by using homogeneous specimens (e.g., cured films) the TBA instrument can be used as a conventional TP to obtain quantitative values of G′ and G″. In the TBA mode the instrument is used principally to measure transition times and transition temperatures.

The equation of motion for a torsion pendulum, in complex format, is [10]:

$$I\ddot{\theta} + \eta\dot{\theta} + KG^*\theta = 0 \tag{1}$$

where I = moment of inertia of the oscillating system
η = air-damping coefficient, which is related to the moving parts of the system
K = factor which depends on the dimensions of the sample
G* = complex shear modulus
θ = angular displacement

The solution of Eq. (1) is:

$$\theta = \theta_0 \exp(-\beta t) \exp(i\omega t) \tag{2}$$

where ω is the angular frequency = 2π/P and β is the decay constant. Differentiating Eq. (2), substituting the results into Eq. (1), and writing G* = G′ + iG″ yields:

$$I(\beta^2 - \omega^2) - \beta\eta + KG' = 0 \tag{3a}$$

$$\eta\omega - 2I\beta\omega + KG'' = 0 \tag{3b}$$

which are obtained by grouping real and imaginary terms.

Now:

$$\theta_n = \theta_0 \exp[t_n(i\omega - \beta)] \tag{4a}$$

$$\theta_{n+1} = \theta_0 \exp[(t_n + P)(i\omega - \beta)] \tag{4b}$$

where t_n is the time required to reach the θ_nth oscillation. Dividing Eq. (4a) by Eq. (4b) yields:

$$\theta_n/\theta_{n+1} = \exp[P(\beta - i\omega] = \exp(P\beta)\exp(-i\omega P)$$
$$= \exp(P\beta)\exp(-i\,2\pi) = \exp(P\beta) \tag{5}$$

Thus, the logarithmic decrement ≡ $\Delta = \ln(\theta_n/\theta_{n+1}) = \beta P$.

Finally, from Eqs. (3a) and (3b):

$$KG' = (4\pi^2 I/P^2)(1 - \Delta^2/4\pi^2 + \Delta P\eta/4\pi^2 I) \tag{6a}$$

$$KG'' = (4\pi I/P^2)(\Delta - \eta P/2I) \tag{6b}$$

If $1 > \Delta \gg \eta P/I$ (the air-damping coefficient is usually negligible):

$$KG' \approx 4\pi^2 I/P^2 \tag{7a}$$

$$KG'' \approx 4\pi I\Delta/P^2 \tag{7b}$$

In a TBA experiment K is unknown, so $G' \propto 1/P^2$, and

$$\Delta \approx KG''/(4\pi I/P^2) = \pi G''/G' = \pi \tan\delta \tag{8}$$

where δ is the phase angle between the cyclic stress and the cyclic strain in the dynamic mechanical experiment. Thus the TBA parameters $1/P^2$ and Δ can be related to the material parameters G′ and G″.

The derivation resulting in Eqs. (6a) and (6b) is based on the assumption that G* is independent of frequency [11]. If the derivation had been performed with the assumption that the dynamic viscosity is frequency-independent, then the minus sign in Eq. (6a) would be replaced by a plus sign [11]. Neither assumption is accurate over a wide range of frequency for high polymers [11]. The plus sign analogue of Eq. (6a) is generally used in this laboratory. The difference between the two approaches is small except in the regions of melting, crystallization and the glass transition, where Δ can be greater than unity.

3.3 Isothermal and Temperature Scans

In order to construct a TTT cure diagram, a series of isothermal cures are performed at different temperatures, and the relative rigidity and logarithmic decrement are recorded vs. time. From each damped wave $1/P^2$ and Δ are extracted; the numerical methods used have been described [12].

In a typical TBA experiment, the glass braid is dipped into a solution containing the reactants, the impregnated braid is clamped to the pendulum, and the pendulum assembly is lowered into the TBA chamber at the cure temperature. T_{cure} is generally above the boiling point of the solvent. The computer program which controls the alignment, intermittent oscillation of the pendulum, and data collection and analysis, is started, and plots of $1/P^2$ and Δ vs. time are produced [12].

The results of a typical isothermal cure are shown in Fig. 3. In general, three events can be discerned in the Δ vs. time plot: a shoulder and two distinct peaks. The first peak is associated with gelation and the second peak with vitrification [2]. The time to gelation has been compared with gel fraction experiments [1-3]; good agreement is generally observed above $_{gel}T_g$. The pre-gel shoulder has been attributed

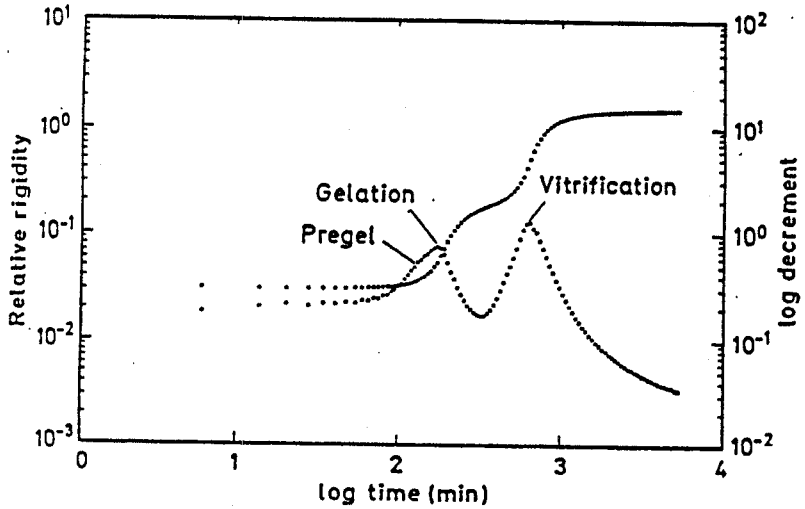

Fig. 3. TBA spectrum during isothermal (125 °C, 75 hr) cure showing changes in the relative rigidity and logarithmic decrement vs. time. Note the location of the pregel shoulder, gelation peak and vitrification peak. The system studied was a difunctional epoxy resin, DER337 [a diglycidyl ether of bisphenol A (DGEBA), Dow Chemical Co.], cured with a stoichiometric amount of a tetrafunctional aromatic amine, TMAB (trimethylene glycol di-p aminobenzoate, Polacure 740M, Polaroid Corp.)

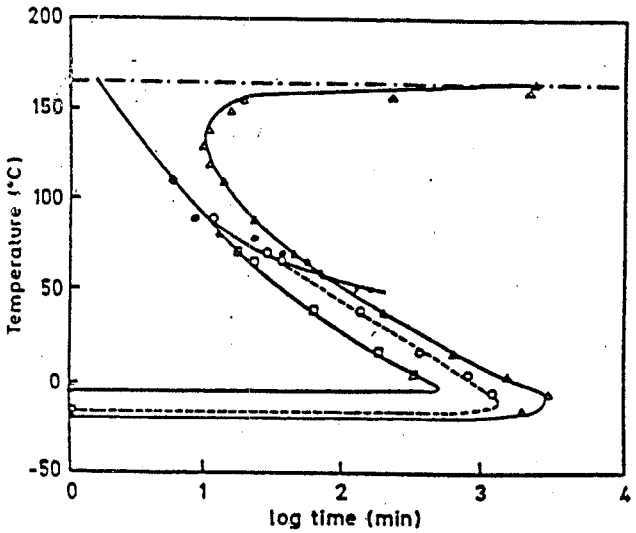

Fig. 4. TTT cure diagram: temperature of cure vs. time to the isoviscous event, gelation and vitrification, including TBA and gel fraction data: □, isoviscous (TBA); ○, gelation (TBA); △, vitrification (TBA); *, gelation (gel fraction). The system studied was a difunctional epoxy resin, Epon 828 (DGEBA, Shell Chemical Co.), cured with a tetrafunctional aliphatic amine, PACM-20. [bis(p-aminocyclohexyl)methane, DuPont]

to an isoviscous event that is due to the interaction of the liquid and the braid [2]. Note that the peaks in the Δ curves are located approximately midway through the transitions in the relative rigidity plots. As the cure reaction proceeds, the relative rigidity (or modulus) increases and eventually appears to level off in the glassy state or in the elastomeric state; distinct loss peaks are associated with the transitions from liquid to sol glass, liquid to sol/gel rubber, and sol/gel rubber to glass.

An example of a TTT cure diagram is shown in Fig. 4, where T_{cure} is plotted vs. the times to gelation and vitrification, as determined by TBA. Note particularly the good agreement, above ${}_{gel}T_g$, between the gel fraction experiments and the TBA results for gelation. (Below ${}_{gel}T_g$, a "liquid-to-rubber" transition is observed in the TBA experiments; the origin of this peak may be due to an interaction between the braid and the polymer) [2]. The vitrification curve is S-shaped, in agreement with the schematic diagram shown in Fig. 1.

Fig. 4 is a TTT diagram for the reaction of a difunctional epoxy with a tetrafunctional aliphatic amine, which is the only system for which the complete TTT diagram (from temperatures less than T_{go} to greater than $T_{g\infty}$) is available. The T_{go} of this system is −19 °C; the amorphous reactants are liquids above this temperature and so the experiments can be performed in the absence of a solvent. Most of the systems studied in this laboratory are very viscous liquids at room temperature and for convenience solvents are used. Only the upper portion of the TTT diagram, above ${}_{gel}T_g$, is usually obtained.

After extended isothermal cure, the system is cooled from T_{cure} to −170 °C, heated from −170 °C to a specified post-cure temperature, and then immediately cooled to −170 °C, all rates of change of temperature being 1.5 K/min. The temperature cycling is continued as long as is desired. The initial scan from −170 °C

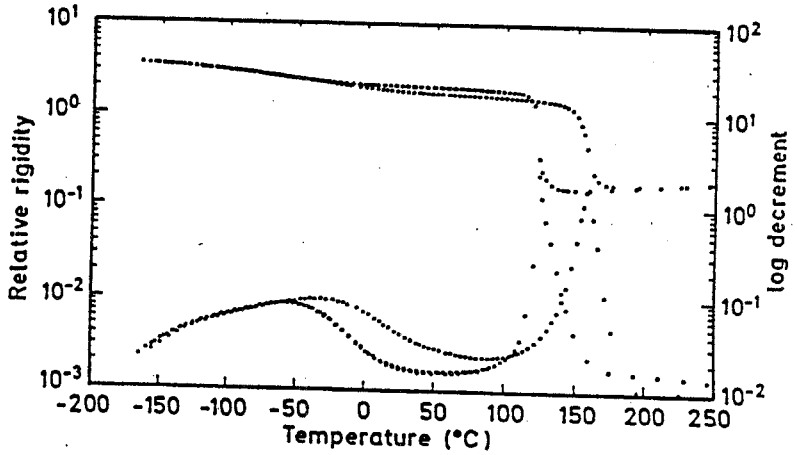

Fig. 5. TBA spectrum after isothermal cure (90 °C, 10^4 min) showing changes in the relative rigidity and logarithmic decrement vs. temperature. Temperature cycle: 90→−170→240→−170 °C, 1.5 °C/min. Note the increase in T_g and T_{gel} with post-cure, but the decrease in the room temperature rigidity (modulus) with post-cure. The system studied was DER337/TMAB (see Fig. 3 caption)

to the post-cure temperature yields the T_g after cure, which is observed to be greater than T_{cure} if the material had vitrified on isothermal cure. The subsequent scan from the post-cure temperature to —170 °C yields a transition temperature, here designated $T'_{g\infty}$, for that particular T_{cure}. $T_{g\infty}$ is obtained by averaging the values of $T'_{g\infty}$ for the different temperatures of cure. The post-cure temperature depends upon the system being investigated. For a variety of tetrafunctional aliphatic and aromatic amines, the post-cure temperature was 240–250 °C for a difunctional epoxy and 280–300 °C for a trifunctional epoxy.

A typical temperature scan of a system after prolonged isothermal cure is shown in Fig. 5. In comparing post-cure behavior with that after cure at T_{cure}, note the increase in T_g as well as in the temperature of the secondary transition (T_{sec}). Also note that the relative rigidity (modulus) of the post-cured material is lower at room temperature (RT) than that of the partially-cured specimen. This behavior is anomalous, because post-cure would be expected to increase the crosslinking, and hence the stiffness of the material. The lower modulus manifests itself in a lower density and greater water absorption at RT for the more highly cured material than for the partially-cured one [13,14].

From plots such as Fig. 5, T_g after cure is determined, and can be plotted vs. T_{cure} (Fig. 6). T_g is observed to exceed T_{cure} primarily because isothermal TBA cures are carried out well beyond the time to the second loss peak in the logarithmic decrement curve (see Fig. 3). If the cure were stopped at the second maximum, then T_g would equal T_{cure} [2]. However, the system would still be reactive because the second loss peak occurs approximately midway through the increase in modulus which accompanies the change from sol/gel rubber to the glass plateau. Similar considerations apply to the conversion of liquid to ungelled glass below ${}_{gel}T_g$. It is convenient in an operational sense to associate the second maximum with vitrification. However, if vitrification is defined to be the point at which chemical reactions are quenched, then a more appropriate determination of the time to vitrification would be when the relative rigidity curve has leveled off with time. In Section 4,

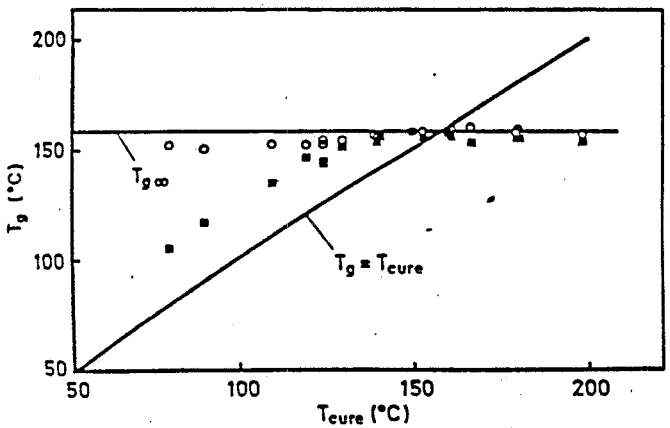

Fig. 6. T_g after prolonged isothermal cure vs. T_{cure}: ■, T_g; ○, $T'_{g\infty}$. $T_{g\infty}$ and $T_g = T_{cure}$ lines are also included. The system studied was DER337/TMAB (see Fig. 3 caption)

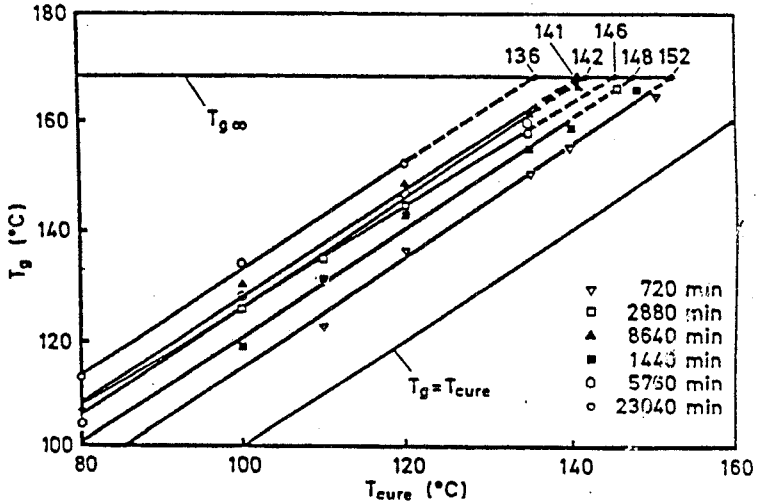

Fig. 7. T_g vs. temperature of cure for different times of cure. The solid lines are the best straight line fits to experimental data (symbols); the dashed lines are the extrapolations to $T_{g\infty}$ to obtain the temperature of cure to reach full cure for the given time. The $T_{g\infty}$ line is also included. The system studied was a difunctional epoxy resin, DER331 (DGEBA, Dow Chemical Co.), cured with TMAB (see Fig. 3 caption). (Peng, X., Gillham, J. K., Ref. [4])

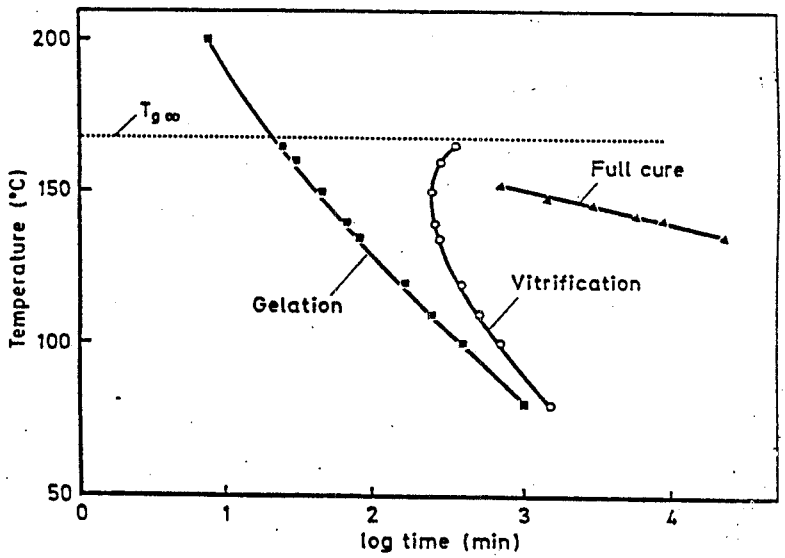

Fig. 8. TTT cure diagram: temperature of cure vs. the times to gelation, vitrification, and full cure. The full cure line is obtained from the extrapolated data of Fig. 7. The system studied was DER331/TMAB (see Fig. 7 caption). (Peng, X., Gillham, J. K., Ref. [4])

vitrification is defined to occur when $T_g = T_{cure}$. Two other reasons for T_g being greater than T_{cure} are: 1) the temperature scan after isothermal cure can promote further reaction as T_g is being measured; and 2) reactions can proceed in the glassy state to an extent determined by the reaction mechanism [4].

In Fig. 6, T_g is shown to be only a function of T_{cure}. However, even for cures carried out well beyond the point where $T_g = T_{cure}$, T_g is actually a function of both the temperature and time of cure [4], as shown in Fig. 7. In Fig. 7, the approximately parallel lines represent a series of isochrones. If each isochrone is extrapolated to $T_{g\infty}$, the isochrone will intersect the horizontal $T_{g\infty}$ line at different values of T_{cure}. For each of these values of T_{cure} (136, 141, 142 °C, etc., Fig. 7), the time for the isochrone is the curing time required to produce full cure (defined to occur when T_g equals $T_{g\infty}$). For example, a T_{cure} of 152 °C, for 720 min, will result in a material with a $T_g = T_{g\infty}$. Plotting T_{cure} obtained from the extrapolation vs. the isochronal cure time on the TTT diagram results in the full cure line (Fig. 8). The full cure line summarizes the time required, at any given T_{cure}, to obtain a material with $T_g = T_{g\infty}$.

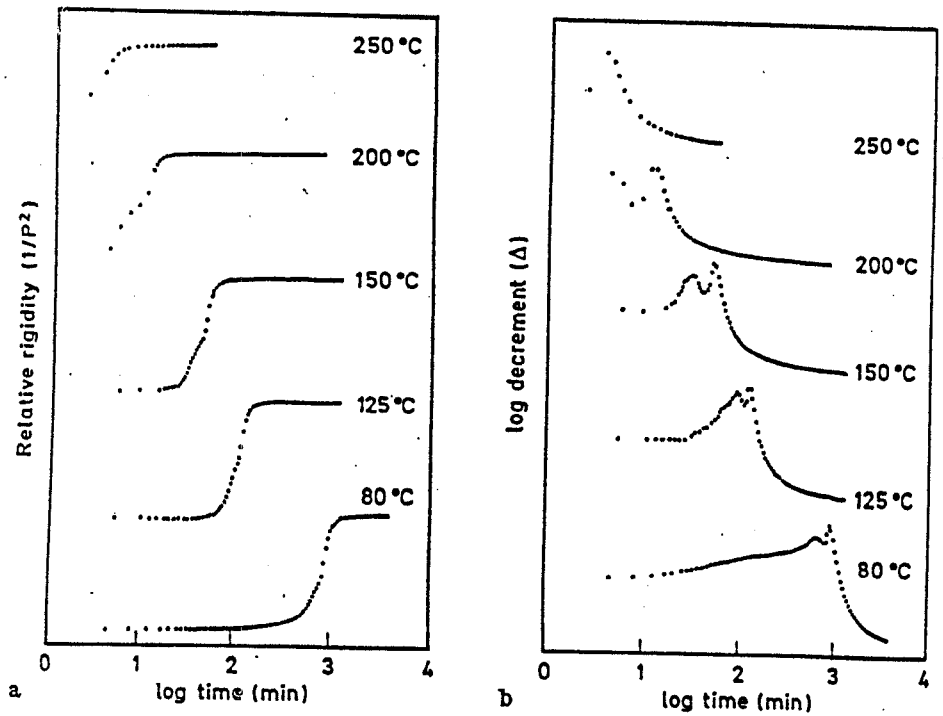

Fig. 9a and b. TBA spectra for a series of isothermal cures showing changes in (a) the relative rigidity and (b) the logarithmic decrement vs. time. Gelation and vitrification are evident in the 80, 125 and 150 °C scans, but only vitrification is observed in the 200 and 250 °C scans. The system studied was a trifunctional epoxy resin, XD7342 [triglycidyl ether of tris(hydroxyphenyl)-methane, Dow Chemical Co.], cured with a tetrafunctional aromatic amine, DDS (diaminodiphenyl sulfone, Aldrich Chemical Co.)

3.4. High T_g Epoxy Resins

For high temperature systems, thermal degradation is an important consideration, and the competition between cure and degradation can prevent full cure, or $T_{g\infty}$, from being reached [3]. For one particular system, with a theoretical $T_{g\infty}$ of 352 °C, isothermal experiments for prolonged times at elevated temperatures can detect degradation events such as devitrification and subsequent revitrification (char formation) [3]. Isothermal plots of relative rigidity and logarithmic decrement, from 80 to 350 °C, for a high T_g epoxy system, are shown in Figs. 9 and 10. For the lower temperatures (Fig. 9), gelation and vitrification peaks are evident in the logarithmic decrement, and the modulus increases as the cure proceeds. At the higher temperatures (Fig. 10) gelation and vitrification occur too rapidly to be measured; however, additional events occur, as evidenced by the maxima in the loss peaks and the associated changes in the modulus. The first maximum (Fig. 10) is associated with a devitrification event (decrease in modulus), whereas the second peak is associated with a revitrification event (increase in modulus). The locus of these events can be placed on the TTT diagram for this system (Fig. 11). Thus, gelation,

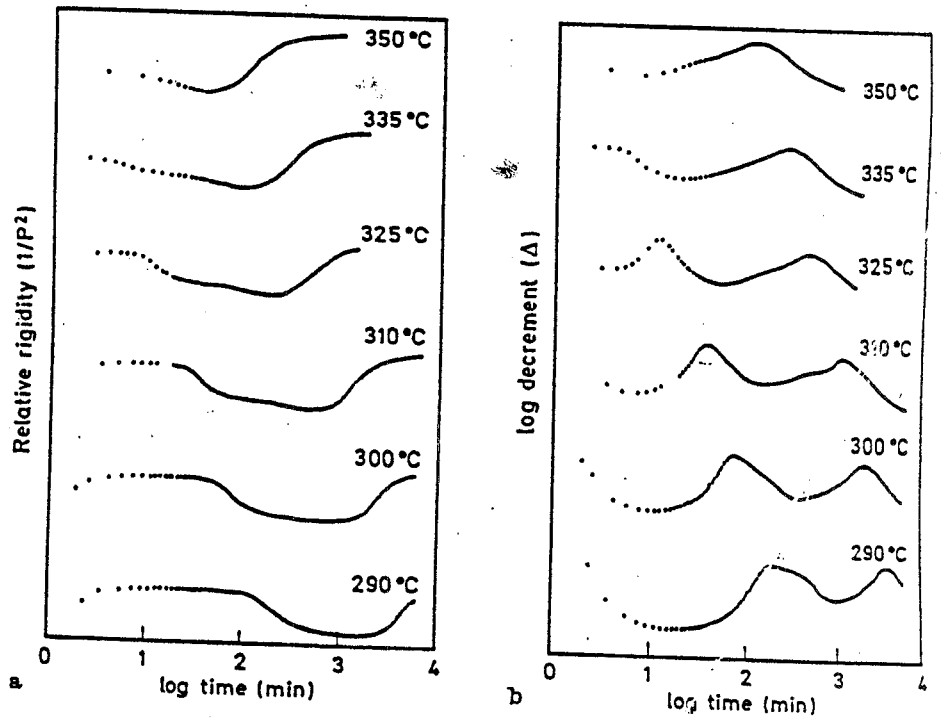

Fig. 10a and b. TBA spectra for a series of isothermal cures showing changes in (a) the relative rigidity and (b) the logarithmic decrement vs. time. Gelation and vitrification are not evident in any of the scans. In the 290–325 °C scans, devitrification and revitrification are observed. In the 335 and 350 °C scans, only the revitrification event (char formation) is observed. The system studied was XD7342/DDS (see Fig. 9 caption)

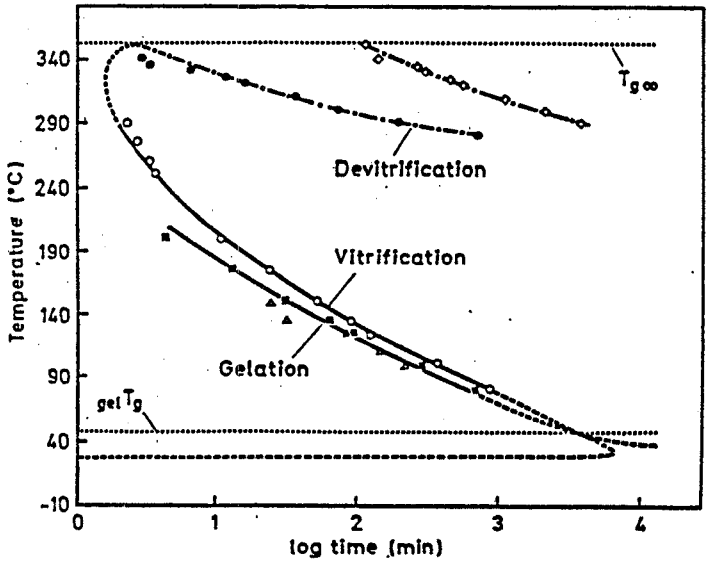

Fig. 11. TTT cure diagram: temperature of cure vs. the times to gelation, vitrification and degradation, including TBA and gel fraction data: ■, gelation (TBA); ○, vitrification; ●, devitrification; ◇, char formation; △, gelation (gel fraction). T_{go}, an estimate of $_{gel}T_g$, and the hypothetical value of $T_{g\infty}$ are included. The system studied was XD7342/DDS (see Fig. 9 caption)

vitrification, devitrification, and revitrification are events that can occur during the isothermal polymerization of high temperature epoxy systems. The TTT cure diagram is a convenient means of summarizing the time-temperature paths of cure that can lead to degradation.

After isothermal cure, temperature scans are conducted in order to measure the T_g after cure and $T_{g\infty}$. However, due to thermal degradation, postcures can lead to lower glass transition temperatures than those obtained after cure. Thus, the determination of $T_{g\infty}$ for high T_g systems is a difficult problem. One approach is to establish a relationship between $T_{g\infty}$ and theoretical crosslink density for systems of lower $T_{g\infty}$ and similar chemical structure, and extrapolate to the system with higher crosslink density, thereby obtaining an estimate of $T_{g\infty}$ [3].

For epoxy systems with moderately high values of $T_{g\infty}$ (220 °C), thermal degradation is still a problem, but full cure in the absence of degradation can be achieved [3]. The TTT diagram for such a system is shown in Fig. 12, where the cure temperature is plotted vs. the times to gelation, vitrification and thermal degradation. Devitrification occurs below $T_{g\infty}$, as in Fig. 12, but other degradation events, including char formation, occur well above $T_{g\infty}$ in the time scale of the experiments.

A comparison of Figs. 11 and 12 also serves to highlight the effect of functionality on cure and properties. The system of Fig. 11 is a trifunctional epoxy cured with a tetrafunctional aromatic amine, whereas the system of Fig. 12 is a difunctional epoxy cured with the same amine. As expected, the more highly functional system has the higher $T_{g\infty}$ and shorter times to gelation; the times to vitrification are also shorter. The difference in these transformation times arises from two factors:

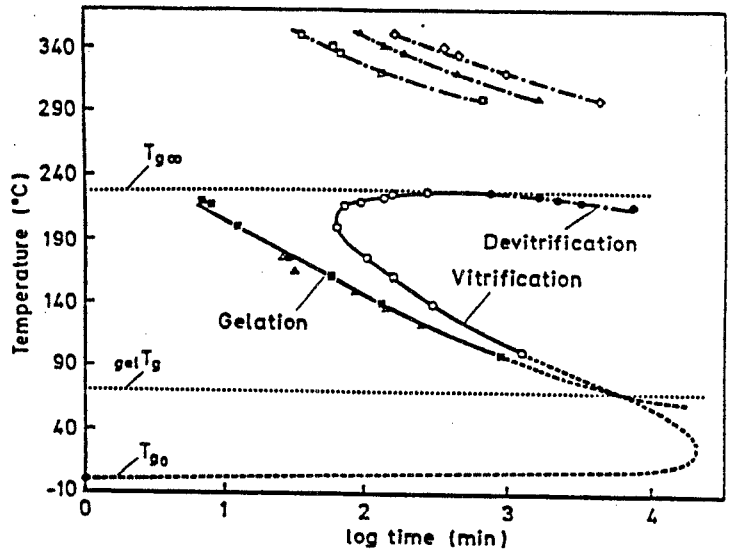

Fig. 12. TTT cure diagram: temperature of cure vs. the times to gelation, vitrification and degradation, including TBA and gel fraction data: ■, gelation (TBA); ○, vitrification; ●, devitrification; □, ▲, degradation events; ◇, char formation; △, gelation (gel fraction). T_{go}, an estimate of $_{gel}T_g$, and the experimental value of $T_{g\infty}$ are included. The system studied was a difunctional epoxy resin, DER332 (DGEBA, Dow Chemical Co.), cured with DDS (see Fig. 9 caption)

1) the extent of conversion at gelation is less for the trifunctional system (Flory's theory [7]), and the extent of conversion at vitrification is also lower [3]; and 2) the concentration of reactants in the trifunctional system is higher than for the difunctional system.

3.5 Rubber-Modified Epoxy Resins

High temperature epoxy resins are brittle materials, and one method of improving their fracture properties is to incorporate reactive liquid rubbers in the formulations [8,15]. In situ phase separation occurs during cure; the cured rubber-modified epoxy resins consist of finely dispersed rubber-rich domains (~0.1–5 μm) bonded to the epoxy matrix. TTT diagrams can be used to compare different rubber-modified systems.

Fig. 13 is a TTT cure diagram of three systems: a neat epoxy resin and the same epoxy modified with two reactive rubbers at the same concentration level. The times to the cloud point, gelation and vitrification are shown for each system. The cloud point is the point of incipient phase separation, as detected by light transmission. The modified system with the longer times to the cloud point and gelation, and the greater depression of $T_{g\infty}$, contains the more compatible of the two rubbers. The difference in compatibility could then be used to account for differences in the volume fractions of the phase separated rubber-rich domains and in the mechanical properties of the neat and the two rubber-modified systems.

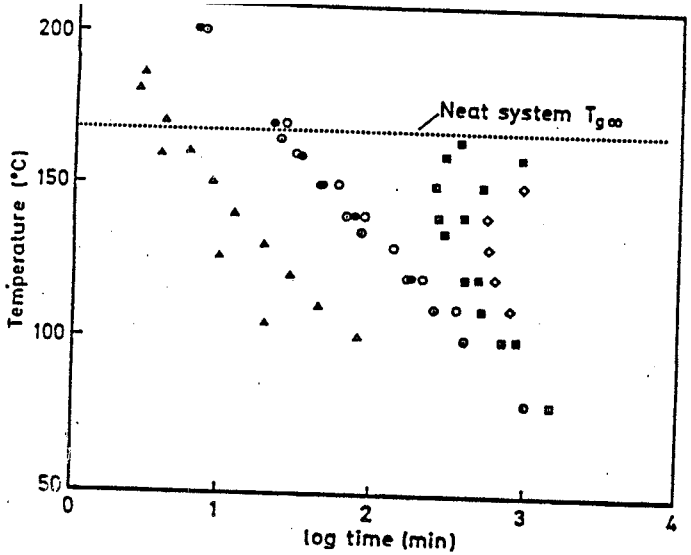

Fig. 13. TTT cure diagram: temperature of cure vs. the times to phase separation (cloud point), gelation and vitrification for a neat and two rubber-modified systems. $T_{g\infty}$ of the neat system is also included. The systems studied were DER331/TMAB: ⊙, gelation; ⊡, vitrification; modified with 15 parts rubber per hundred parts epoxy: 1) prereacted carboxyl-terminated butadiene-acrylonitrile (CTBN) copolymer containing 17% acrylonitrile (K-293, Spencer Kellog Co.): ▲, phase separation; ●, gelation; ■, vitrification, and 2) polytetramethylene oxide terminated with aromatic amine (ODA2000, Polaroid Corp.): △, phase separation; ○, gelation; ◇, vitrification. (DER331/TMAB/K-293 data from Ref. [8])

Isothermal TBA scans of rubber-modified systems show no evidence of phase separation, and they only differ from the neat systems in terms of the transition times. In the subsequent temperature scans, however, the presence of the rubber-rich domains is evident by the distinct loss peaks at the T_g of the rubber (~−50 °C) (Fig. 14). The relative rigidity plots are qualitatively similar to those seen previously (e.g., Fig. 5), including the inversion of the moduli at RT.

In this Section, an experimental approach for constructing isothermal TTT cure diagrams has been described, TTT diagrams of representative epoxy systems including high T_g and rubber-modified epoxy resins have been discussed, and perturbations to the TTT cure diagram due to thermal degradation and rubber modification have been illustrated.

4 Modeling the TTT Cure Diagram

Although different aspects of the isothermal TTT cure diagram have been presented in this review from an experimental point of view, this section will present some recent work that has attempted to model the cure process. Only the gelation and vitrification processes are examined, and the complicating effects of thermal degrada-

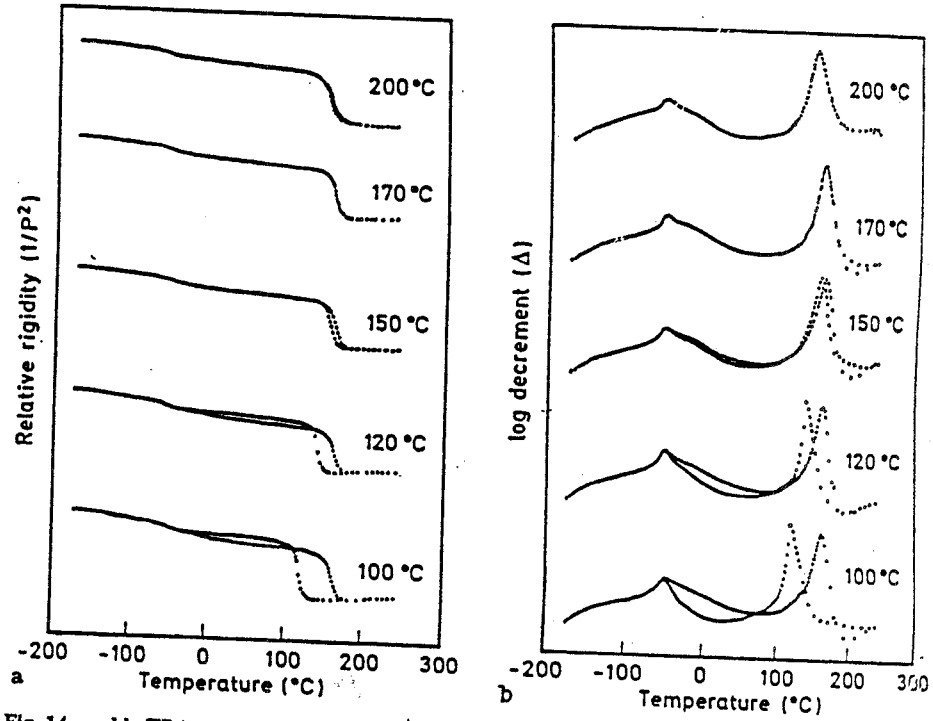

Fig. 14a and b. TBA spectra after isothermal cure showing changes in (a) the relative rigidity and (b) the logarithmic decrement vs. temperature: T_{cure}→170→240→−170 °C, 1.5 °C/min. Note presence of rubber T_g peak at about −50 °C. The system studied was DER331/TMAB/K-293 (see Fig. 13 caption)

tion, rubber modification, and viscosity (diffusion control) are ignored. More sophisticated models could incorporate the refinements.

During isothermal polymerization below $T_{g\infty}$, the molecular weight and T_g increase, and eventually T_g will equal T_{cure}. The main purpose of this section is to discuss the calculation of the time to vitrification, where vitrification is defined to occur when T_g equals T_{cure}. The concepts of vitrification and the TTT cure diagram are extended to linear systems for both step growth and chain reaction mechanisms, although most of the discussion will focus on the nonlinear step growth case, of which the cure of epoxy resins is an example.

The calculation of the time to gelation is straightforward if gelation is assumed to be an isoconversion state [7], and if the kinetics of the reaction are known. The rate of reaction in general is:

$$-dc/dt = kf(c, c_1, c_2, \ldots) \tag{9}$$

where c is the concentration of the reactant under consideration, k is the temperature-dependent rate constant, and c_1, c_2, ... are the concentrations of other reactants in the system. $f(c, c_1, c_2, \ldots)$ is a function of the reaction mechanism and the extent of conversion. For the simple case of two reactants in stoichiometric ratio, as is

considered in this section, $f(c, c_1, c_2, ...)$ can be reduced to $f(c)$. Substituting $c = c_0(1 - p)$ into Eq. (9), and integrating yields:

$$kt = \int c_0 \, dp/f[c_0(1 - p)] \tag{10}$$

For example, if the reaction is first order, $f[c_0(1 - p)] = c_0(1 - p)$, and $kt = -\ln(1 - p)$, where p is the extent of reaction.

The conversion at gelation is generally assumed to follow from Flory's theory (7):

$$p_{gel} = 1/(f - 1)^{1/2} \tag{11}$$

where f is the functionality of the multifunctional unit in a nonlinear reaction. Equation (11) is valid for the stoichiometric reaction of a multifunctional reactant A_f with a difunctional reactant B_2. For the typical case of a difunctional material cured with a tetrafunctional material, $f = 4$ and $p_{gel} = 0.577$. Experimental values of p_{gel} are usually observed to be greater than the predicted values because of non-idealities relative to the theory, such as intramolecular ring formation and unequal reactivities of the same functional groups.

Equations (9) and (10) assume that the reactions are not diffusion controlled and only one temperature-independent reaction mechanism is operable. Epoxy thermosetting reactions are actually complex, and complicated kinetic expressions and competing reaction mechanisms have been proposed [16].

Whereas the calculation of the time to gelation is relatively simple, the calculation of the time to vitrification (t_{vit}) is not so elementary. The critical point is to obtain a relationship between T_g and the extent of conversion at T_g (p_{vit}). Once the conversion at T_g is known, then the time to vitrification can be calculated from the kinetics of the reaction. Two approaches have been examined: one calculates t_{vit} based on a relationship between T_g and p_{vit} in conjunction with experimental values of p_{vit} [6,17]; the other approach formulates the T_g vs. p_{vit} relationship from equations in the literature relating T_g to molecular weight and molecular weight to extent of reaction [18,19].

The first method of calculating t_{vit} is based on an equation from DiBenedetto, as presented in Nielsen [20]:

$$(T_g - T_{g\infty})/T_{go} = (\varepsilon_x/\varepsilon_M - F_x/F_M)\, p_{vit}/[1 - (1 - F_x/F_M)\, p_{vit}] \tag{12}$$

where $\varepsilon_x/\varepsilon_M$ = ratio of lattice energies for crosslinked and uncrosslinked polymers, F_x/F_M = corresponding ratio of segmental mobilities.

In DiBenedetto's original equation, T_{go} represented the glass transition temperature of a polymer of the same chemical composition as the crosslinked polymer except without the crosslinks, and X_c was used instead of p_{vit}, where X_c is the mole fraction of monomer units which are crosslinked in the polymer. Thus, the original equation was applicable to the crosslinking of long linear polymers.

In order to use Eq. (12) values of $\varepsilon_x/\varepsilon_M$ and F_x/F_M must be determined. Adabbo and Williams [17] assumed $\varepsilon_x/\varepsilon_M = 1$, and they found $F_x/F_M = 0.733$ was an acceptable value for fitting p_{vit} vs. T_g data for several epoxy systems. Enns and Gillham [6] fitted

Eq. (12) to experimental p_{vit} vs. T_g data, for one particular system, with a non-linear least squares routine and found $\varepsilon_x/\varepsilon_M = 0.34$ and $F_x/F_M = 0.19$.

With values of $\varepsilon_x/\varepsilon_M$ and F_x/F_M, it is a simple matter to calculate p_{vit} at any value of T_g ($= T_{cure}$), and then determine the time to vitrification from an assumed kinetic rate law. Using first order kinetics, which seemed to fit the extent of conversion vs. time data, the temperature of cure vs. the times to gelation and vitrification are shown in Fig. 15. The model fits the data well at low temperatures but appears to

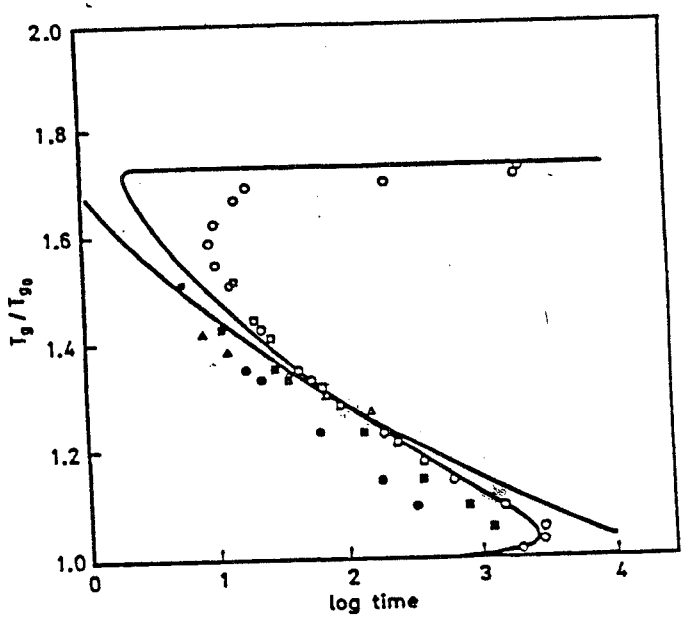

Fig. 15. TTT cure diagram: T_g/T_{go} vs. times to gelation and vitrification. Theoretical (solid lines): First-order kinetics using the following parameters: $T_{go} = -19$ °C; $T_{g\infty} = 166$ °C; $\varepsilon_x/\varepsilon_M = 0.34$; $F_x/F_M = 0.19$; $E_a = 12.6$ kcal/mole; $A = 4.5 \times 10^6$ min^{-1}; $p_{gel} = 0.75$; $T_g = 49$ °C. Experimental: ●, pregel (TBA); ■, gelation (TBA); ○, vitrification (TBA); □, diffusion control (infrared spectroscopy); △, gelation (gel fraction). The system studied was Epon 828/PACM-20 (see Fig. 4 caption)

fail at high temperatures, where the time to vitrification is very short. In a TBA experiment the system generally requires several minutes to equilibrate thermally, which could account for the lack of agreement at high temperature.

Data for the time to the onset of diffusion control, as determined by infrared spectroscopy, are also included in Fig. 15. The time to diffusion control was selected as the point at which the extent of conversion vs. time data, plotted for first order kinetics, deviated from linearity. The onset of diffusion control corresponds with vitrification, as determined by TBA, for the system of Fig. 15 [6].

In the above model, data for the extent of reaction at vitrification are needed. These data were obtained using infrared spectroscopy. The extent of conversion of the epoxy group was monitored as a function of time at a series of temperatures. A corresponding set of TBA experiments was performed, and the time to vitrification data were

superimposed on the extent of conversion data, at the different temperatures, to obtain the conversion at vitrification.

The second approach attempts to predict p_{vit}, and then calculates t_{vit} from those predictions [18,19]. In addition, this second model can be extended easily to linear polymerizations for different reaction mechanisms.

Several relationships are needed to calculate t_{vit}. These are:

i) $T_{cure} = T_g$
ii) T_g vs. molecular weight or crosslink density
iii) molecular weight or crosslink density vs. extent of reaction
iv) extent of reaction vs. time.

Molecular weight is used for linear systems, and for thermosetting systems that have not crosslinked (i.e., below ${}_{gel}T_g$). There are four cases of importance-linear systems for step growth and chain reaction mechanisms, and nonlinear systems for step growth and chain reaction mechanisms — but only examples of the first three are discussed here.

For linear systems, an equation relating T_g and the number average molecular weight (M_n) is [21–23]:

$$1/T_g = 1/T_{g\infty} + K/M_n \tag{13}$$

where K is a constant. This Equation is applicable over a wide range of values of molecular weight.

For nonlinear systems, two regimes are distinguishable: (1) vitrification that occurs below ${}_{gel}T_g$; and (2) vitrification that occurs above ${}_{gel}T_g$. Below ${}_{gel}T_g$ the systems will vitrify without gelling, so the material is not crosslinked. Above ${}_{gel}T_g$, both crosslinked and uncrosslinked material are present at vitrification.

Eq. (13) was used to relate T_g and M_n below ${}_{gel}T_g$, even though the material is branched at vitrification. (An estimate of $T_{g\infty}$ for uncrosslinked material was obtained by using Eq. (13) at T_{g0} and ${}_{gel}T_g$.) A more appropriate expression, which attempts to account for the effect of branching on T_g, has been proposed [24].

Above ${}_{gel}T_g$, T_g must be related to the molecular weight of the sol fraction and the crosslink density of the gel fraction. If the system is considered to be a miscible binary mixture of sol and gel fractions, then [25]:

$$T_g = w_s T_{gs} + w_g T_{gg} + I w_s w_g \tag{14}$$

where T_{gs}, T_{gg} = glass transition temperatures of sol and gel, respectively; w_s, w_g = weight fractions of sol and gel, respectively; and I = an interaction parameter. T_{gs} is considered to be given by Eq. (13), where M_n is now the molecular weight of the sol fraction only. T_{gg} is given by [19]:

$$T_{gg} = {}_{gel}T_g + K_x[X] \tag{15}$$

where K_x is a constant and [X] the concentration of crosslinks in moles of crosslinks

per volume of polymer. A linear relationship between T_{gg} and [X] is one of several proposed [8,21,26].

In general, for uncrosslinked step growth systems, for the reaction of an f-functional reactant A_f with an h-functional reactant B_h, M_n is related to the extent of reaction p by [27]:

$$M_n = (M_{A_f}A_f + M_{B_h}B_h)/(A_f + B_h - p_A f A_f) \tag{16}$$

where M_{A_f}, M_{B_h} are molecular weights of reactants A_f and B_h, respectively; A_f, B_h are moles of components A_f and B_h, respectively; and p_A is the extent of reaction of A_f. For the linear step-growth polymerization of A_2 with B_2, in stoichiometric ratio, $M_n = (M_A + M_B)/[2(1 - p)]$. For the nonlinear step-growth polymerization of A_4 with $2B_2$, $M_n = (M_A + 2M_B)/(3 - 4p)$.

For the case of linear, chain growth polymerization, the experimental and computed number average molecular weights are usually given for the polymeric portion of the reacting mixture, rather than for the entire reactor contents. Since the T_g in bulk polymerization is affected by residual monomer as well as polymer, a relationship between total M_n (i.e., monomer with polymer) and p is needed. The contribution of initiator is neglected, and the concentration of growing chains is negligible. Since M_n is defined as the total weight of material divided by the total number of moles (monomer plus polymer), and the number of moles of polymer is given by:

$$\text{moles polymer} = \frac{\text{(moles of monomer in polymer)}}{\text{(moles of monomer/polymer)}} = \frac{p}{\langle X_n \rangle} \tag{17}$$

where $\langle X_n \rangle$ is the cumulative number average degree of polymerization of the polymer, then:

$$M_n = M_0/[(1 - p) + p/\langle X_n \rangle] \tag{18}$$

where M_0 is the monomer molecular weight.

For the nonlinear step growth case above ${}_{gel}T_g$, the crosslink density must be related to p. A relevant model, based on calculating the probabilities of finite chains being formed, has been published [28]. For the reaction of $A_4 + 2B_2$ (e.g., tetrafunctional amine + difunctional epoxy), A_4 is considered to be an effective crosslinking site if three or more of its arms lead out to the infinite network. The probability of finding an effective crosslink is related to one minus the probability of a randomly chosen A_4 leading to the start of a finite chain, which in turn is related to the extent of reaction. Application of this procedure to the system of Fig. 15 has been presented in detail [19]. The more complicated reaction of a tetrafunctional amine with a trifunctional epoxy was also considered [19].

The last step in this second model is to relate the extent of reaction at vitrification to time. For the step growth mechanism, for both linear and nonlinear systems, nth order kinetics were assumed [29,30]:

$$-dc/dt = kc^n \tag{19}$$

For the linear chain reaction case, a free radical kinetic mechanism (e.g., polymeriza-

tion of styrene) was used as an example. In this the rate of polymerization is given by [31,32]:

$$R_p = -d[M]/dt = k_p[M]\,(fk_d[I]/k_t)^{1/2} \qquad (20)$$

where $[M]$ = monomer concentration at time t
k_p = propagation rate constant
f = initiator efficiency
k_d = initiator decomposition rate constant
$[I]$ = initiator concentration at time t
k_t = termination rate constant

If first order decomposition of the initiator is assumed, and from $[M] = [M]_0\,(1 - p)$, integrating Eq. (20) over time yields:

$$-\ln(1 - p) = 2k_p(f[I]_0/k_dk_t)^{1/2}\,(1 - \exp(-k_dt/2)) \qquad (21)$$

where $[I]_0$ is the initial initiator concentration and $[M]_0$ is the initial monomer concentration.

For the linear free radical case, one additional equation is needed, relating $\langle X_n \rangle$ to the other variables [32]:

$$\langle X_n \rangle = ([M]_0 - [M])/(f\{[I]_0 - [I]\}) = [M]_0\,p/(f[I]_0\{1 - \exp(-k_dt)\}) \qquad (22)$$

In Eq. (22), termination by combination was used.

The time to vitrification, as a function of reaction temperature, can now be solved for each of the three cases considered. The only case for which experimental data are available for t_{vit} is the nonlinear step growth case. Combining Eqs. (13)–(16), (19), and those relating the crosslink density to p, results in the plot of T_{cure} vs. t_{vit} shown in Fig. 16. The system used was the same one used in Fig. 15. Different values of the reaction order (n) were used in Fig. 16. The value of k obtained for n = 1 was used for all values of n. The fit is not entirely satisfactory, but the lack of an accurate kinetic model mitigates against a good fit. The calculated time to vitrification curve is S-shaped, as is seen experimentally.

The model predictions of the extents of reaction at vitrification vs. reaction temperature are compared to the experimental values in Fig. 17. The model predictions are too low, and the inherent simplifications in the model could account for some of the discrepancy. These simplifications include [28]: all functional groups of the same type are equally reactive; all groups react independently of one another; and no intramolecular reactions occur in finite species.

The model was also applied to the reaction of a tetrafunctional amine with a trifunctional epoxy, denoted $A_4 + 4/3B_3$, and was compared with available data (Fig. 18). An approximate value of k was obtained from the times to gelation. This model appears to provide a reasonable framework within which the vitrification process for nonlinear systems can be discussed.

Time to vitrification data for the other two cases are not available. For a hypothetical linear step growth reaction of $A_2 + B_2$, with reasonable values of M_A, M_B,

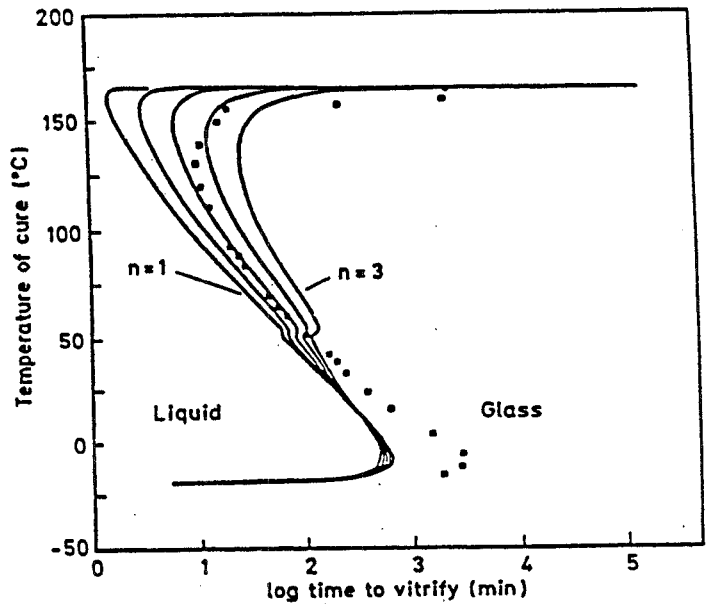

Fig. 16. Reaction temperature vs. time to vitrify for nonlinear step-growth polymerization ($A_4 + 2B_2$): nth-order kinetics for n = 1 to 3 in increments of 0.5 using the following parameters: $T_{g0} = -19$ °C; $_{gel}T_g = 50$ °C; $T_{g\infty} = 166$ °C; $E_a = 12.6$ kcal/mole; $A = 4.51 \times 10^6$ min^{-1}; $M_A = 210$ gm/mole; $M_B = 382$ gm/mole. Data (squares) are from the study of Epon 828/PACM-20 [6]. (See Fig. 4 caption for description of materials.) [Aronhime, M. T., Gillham, J. K.: J. Coat. Tech. *56* (718), 35 (1984)]

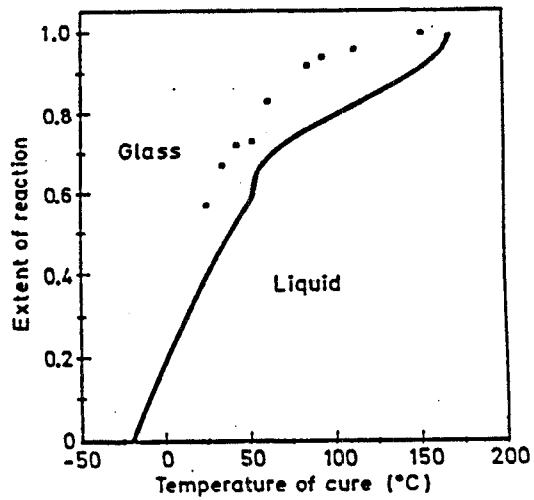

Fig. 17. Extent of reaction at vitrification vs. reaction temperature for nonlinear step-growth polymerization ($A_4 + 2B_2$). All kinetic orders have the same p at vitrification. For model parameters and system, see Fig. 16 caption. [Aronhime, M. T., Gillham, J. K.: J. Coat. Tech. *56* (718), 35 (1984)]

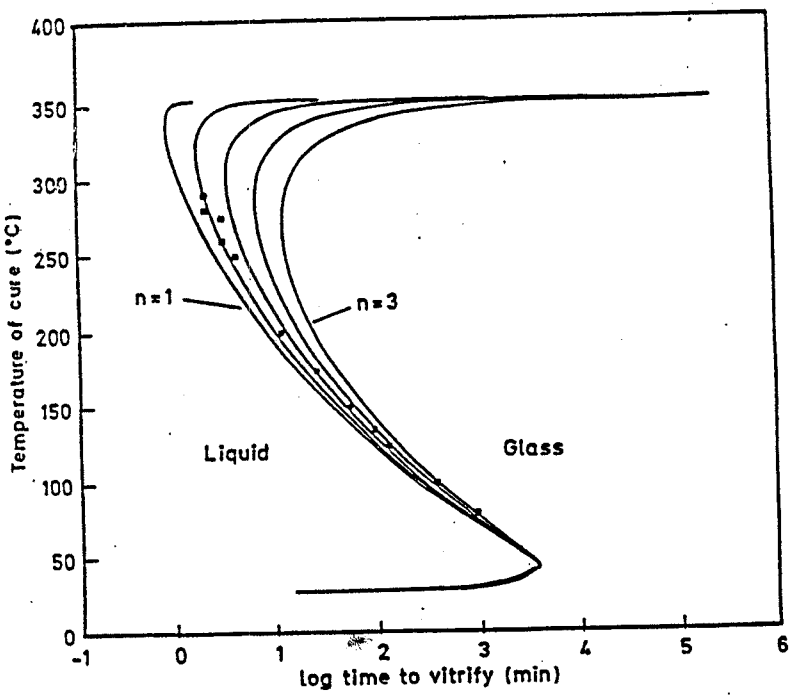

Fig. 18. Reaction temperature vs. time to vitrify for nonlinear step-growth polymerization ($A_4 + {}^4/_3B_3$): nth-order kinetics for n = 1 to 3 in increments of 0.5 using the following parameters: T_{go} = 28 °C; T_g = 42 °C; $T_{g\infty}$ = 352 °C; E_a = 13.3 kcal/mole; A = 2.49 × 10^5 min^{-1}; M_A = 448.4 gm/mole; M_B = 486 gm/mole. Data (squares) are from the study of XD7342/DDS [3]. (See Fig. 9 caption for description of materials.) [Aronhime, M. T., Gillham, J. K.: J. Coat. Tech. *56* (718), 35 (1984)]

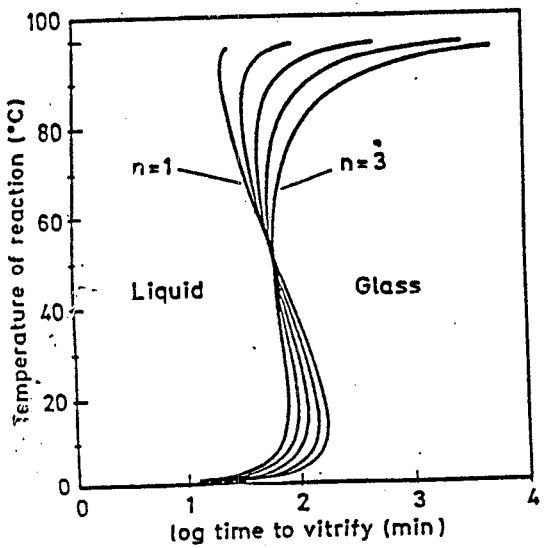

Fig. 19. Reaction temperature vs. time to vitrify for linear step-growth polymerization: nth-order kinetics, for n = 1 to 3 in increments of 0.5 using the following parameters: T_{go} = 0 °C; $T_{g\infty}$ = 100 °C; E_a = 12.6 kcal/mole; A = 4.51 × 10^6 min^{-1}; M_A = 200 gm/mole; M_B = 400 gm/mole. [Aronhime, M. T., Gillham, J. K.: J. Coat. Tech. *56* (718), 35 (1984)]

T_{go}, $T_{g\infty}$, and k, the temperature of reaction vs. time to vitrification is S-shaped (Fig. 19). However, a change in the activation energy of the reaction, to a value less than some critical value ($E_a < E_{a,crit}$), where $k = A \exp(-E_a/RT)$, results in the sigmoidally-shaped vitrification curves included in Fig. 20. E_a was selected to be less than $E_{a,crit}$ for n = 2; this value of E_a was used for all values of n. In the expression for k, A is the pre-exponential factor, R is the gas constant, and T is the absolute temperature. Thus, in principle the time to vitrification curve need not be S-shaped.

For the linear-free radical case, the time to vitrification is affected by the initial initiator concentration (Fig. 21). The vitrification curves are again S-shaped. For this case, the same values of k_p, k_t, and k_d were used throughout the course of the reaction, although it is well known that the termination reaction becomes diffusion controlled at fairly low degrees of conversion [33].

Due to the nature of free radical polymerization, i.e., the reacting system is essentially a binary mixture composed of monomer and high polymer, another approach was used to calculate p_{vit}, and therefore t_{vit} [18,19]. This alternate method is based on the free volume theory, which predicts a relationship between T_g and the volume fractions of polymer and monomer in a binary system [34,35]:

$$T_g = (\alpha_p \varphi_p T_{gp} + \alpha_m (1 - \varphi_p)\, T_{gm}) / (\alpha_p \varphi_p + \alpha_m (1 - \varphi_p)) \qquad (23)$$

where α = volume coefficient of expansion of liquid minus volume coefficient of

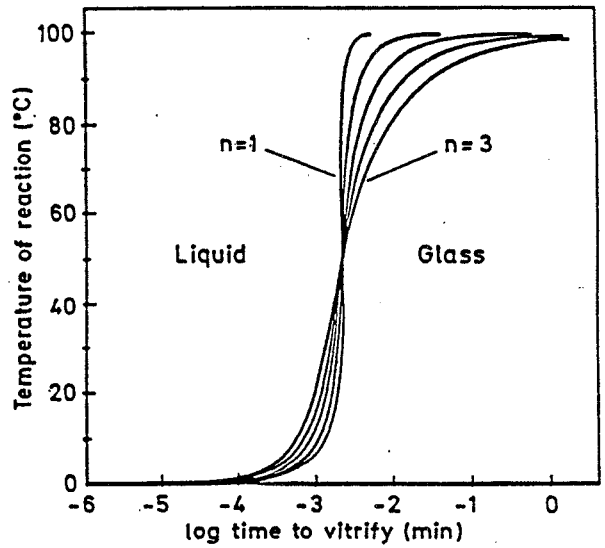

Fig. 20. Reaction temperature vs. time to vitrify for linear step-growth polymerization: nth-order kinetics, for n = 1 to 3 in increments of 0.5 using the following parameters: T_{go} = 0 °C; $T_{g\infty}$ = 100 °C; E_a = 6 kcal/mole; A = 4.51 × 10^6 min^{-1}; M_A = 200 gm/mole; M_B = 400 gm/mole. [Aronhime, M. T., Gillham, J. K.: J. Coat. Tech. *56* (718), 35 (1984)]. [In this case, E_a is less than $E_{a,crit}$ (see text)]

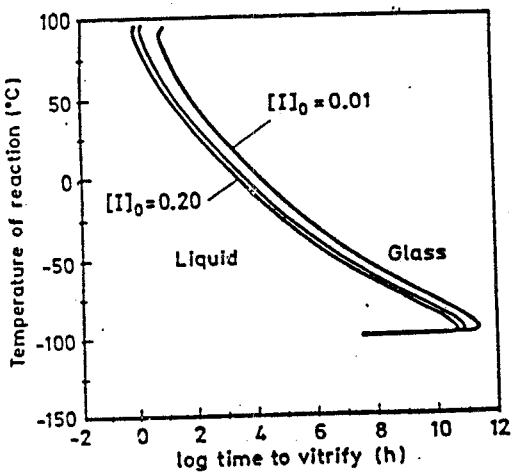

Fig. 21. Reaction temperature vs. time to vitrify for linear free-radical polymerization (styrene) for $f = 0.5$ and $[I]_0 = 0.01$, 0.10 and 0.20 mole/l using the following parameters: $T_{g0} = -100$ °C; $T_{g\infty} = 100$ °C; M_n (monomer) = 104 gm/mole; $k_p = (1.62 \times 10^{10}\ \mathrm{l\ mole^{-1}\ hr^{-1}}) \times \exp(-6.21\ \mathrm{kcal\ mole^{-1}}/RT)$; $k_t = (2.088 \times 10^{11}\ \mathrm{l\ mole^{-1}\ hr^{-1}}) \times \exp(-1.91\ \mathrm{kcal\ mole^{-1}}/RT)$; $k_d = (2.725 \times 10^{17}\ \mathrm{hr^{-1}}) \exp(-29.71\ \mathrm{kcal} \times \mathrm{mole^{-1}}/RT)$. [Aronhime, M. T., Gillham, J. K.: J. Coat. Tech. *56* (718), 35 (1984)]

expansion of glass, φ = volume fraction, and the subscripts p and m refer to polymer and monomer, respectively. From Eq. (23):

$$\varphi_p = [\alpha_m(T_{gm} - T_g)]/[\alpha_p(T_g - T_{gp}) + \alpha_m(T_{gm} - T_g)] \tag{24}$$

From a mass balance on the polymer and monomer:

$$\varphi_p = (p/\varrho_p)/[(1 - p)/\varrho_m + p/\varrho_p] \tag{25}$$

where ϱ = density. Thus:

$$p = 1/[(1/\varphi_p - 1)\,\varrho_m/\varrho_p + 1] \tag{26}$$

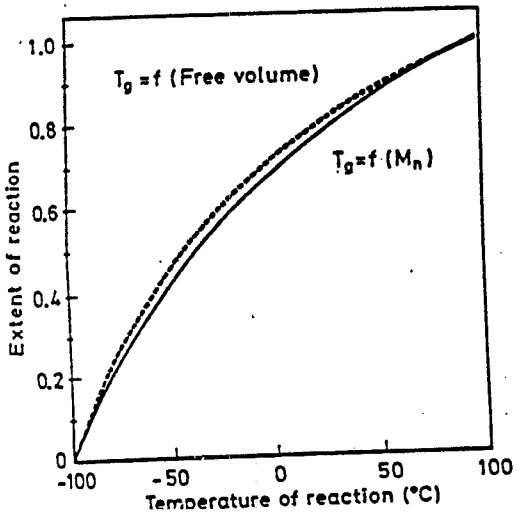

Fig. 22. Extent of reaction at vitrification vs. reaction temperature for linear free-radical polymerization (styrene) for $f = 0.5$ and $[I]_0 = 0.10$ mole/l. The solid line is for the results from the T_g-molecular weight model [Eq. (21)]; the dashed line is for the results from the free volume theory [Eq. (26)]. [Aronhime, M. T., Gillham, J. K.: J. Coat. Tech. *56* (718), 35 (1984)]

The values of p_{vit} from Eq. (26) are compared with the values calculated from Eq. (21) (Fig. 22), and show good agreement over the entire temperature range.

In this section, two different approaches to calculating the time to vitrification on isothermal polymerization have been examined. The first approach used an existing relationship between T_g and p_{vit}, and the time was calculated from an assumed rate law. The second method derived the values of p_{vit} from basic equations in polymer science and then used an assumed rate law to calculate the time.

Neither model is entirely satisfactory in fitting the experimental data. The complexity of epoxy curing reactions contributes to the discrepancies. Many different mechanisms have been proposed [6,36,37]. The diffusion controlled nature of the reactions as vitrification is approached is another complicating factor. Both models do predict the S-shaped vitrification curve, and the second model extends the concept of the TTT diagram to linear systems.

5 Conclusions

A time-temperature-transformation (TTT) isothermal cure diagram has been developed to provide an intellectual framework for understanding and comparing the cure of thermosetting systems. The times to gelation, vitrification, thermal degradation, and phase separation can be conveniently summarized on the TTT diagram. The TTT diagram can also be extended to linear systems, except that these systems do not undergo gelation.

In order to obtain a TTT cure diagram, the cure process must be monitored from the liquid region, through the sol/gel rubber region, and into the glass region. The torsional braid analyzer (TBA) is an instrument capable of following the entire cure process. The TBA, unlike the conventional torsion pendulum from which it was derived, uses supported specimens, and thus can monitor properties above load limiting transition temperatures.

During isothermal cure, maxima in the logarithmic decrement are associated with gelation and vitrification. The times to gelation as measured by TBA correlate for the most part with times as measured in gel fraction experiments. The loss peak associated with vitrification occurs when $T_g = T_{cure}$ and the modulus is midway between the liquid, or sol/gel rubber, and glass plateaus. The chemical reactions are quenched not when $T_g = T_{cure}$, but when the modulus levels off. The TTT diagram is constructed by plotting the cure temperature vs. the times to gelation and vitrification.

For high temperature and rubber-modified epoxy resins, thermal degradation events and the cloud point curve are included on the diagrams, respectively. Two degradation events have been assigned: devitrification, or a glass-to-rubber event; and revitrification, which is associated with char formation. The cloud points and depressions of $T_{g\infty}$ for different rubber-modified epoxies can be compared and related to volume fractions of the second phase and to the mechanical properties of the cured materials.

Two models for calculating the time to vitrification on isothermal polymerization have been discussed. One model is based on an existing relationship between T_g

and the extent of conversion at T_g. Data for the extent of conversion at vitrification must be available to use this approach. The second model calculates p_{vit} from several relationships between T_g and molecular weight, and molecular weight and extent of reaction. The second approach can be extended naturally to linear systems. Both models use an assumed kinetic mechanism to calculate the time to vitrification, and an S-shaped time to vitrification curve is predicted.

Acknowledgements: The research covered by this review has been supported by the Army Research Office and the Office of Naval Research.

6 References

1. Enns, J. B., Gillham, J. K.: ACS Adv. Chem. Ser. 203, 27 (1983)
2. Gillham, J. K.: in Developments in Polymer Characterisation-3, J. V. Dawkins, Ed., p. 159, Applied Science, London 1982
3. Chan, L. C., Naé, H. N., Gillham, J. K.: J. Appl. Polym. Sci. *29*, 3307 (1984)
4. Peng, X., Gillham, J. K.: J. Appl. Polym. Sci., J. Appl. Polym. Sci. *30*, 4685 (1985)
5. Chadwick, G. A.: Metallography of Phase Transitions, Crane, Russak & Co., Inc., N.Y. 1972
6. Enns, J. B., Gillham, J. K.: J. Appl. Polym. Sci. *28*, 2567 (1983)
7. Flory, P. J.: Principles of Polymer Chemistry, Cornell University, Ithaca, N.Y. 1953
8. Chan, L. C., Gillham, J. K., Kinloch, A. J., Shaw, S. J.: ACS Adv. Chem. Ser. 208, 235 (1984)
9. Gillham, J. K.: AIChE J. *20* (6), 1066 (1974)
10. Read, B. E., Dean, G. D.: The Determination of Dynamic Properties of Polymers and Composites, pp. 54–56, John Wiley & Sons, N.Y. 1978
11. Nielsen, L. E.: Mechanical Properties of Polymers, pp. 194–5, Reinhold Publishing Corp., N.Y. 1962
12. Enns, J. B., Gillham, J. K.: ACS Symp. Ser. 197, 329 (1982)
13. Enns, J. B., Gillham, J. K.: J. Appl. Polym. Sci. *28*, 2831 (1983)
14. Aronhime, M. T., Peng, X., Gillham, J. K., Small, R. D.: J. Appl. Polym. Sci., in press
15. Chan, L. C., Gillham, J. K., Kinloch, A. J., Shaw, S. J.: ACS Adv. Chem. Ser. 208, 261 (1984)
16. Osinski, J. S., Manzione, L. T.: ACS Symp. Ser. 221, 263 (1983)
17. Adabbo, H. E., Williams, R. J. J.: J. Appl. Polym. Sci.: *27*, 1327 (1982)
18. Aronhime, M. T., Gillham, J. K.: J. Appl. Polym. Sci. *29*, 2017 (1984)
19. Aronhime, M. T., Gillham, J. K.: J. Coat. Techn. *56* (718), 35 (1984)
20. Nielsen, L. E.: J. Macromol. Sci.-Revs. Macromol. Chem. *C3* (1), 69 (1969)
21. Fox, T. G., Loshaek, S.: J. Polym. Sci. *15*, 371 (1955)
22. Ueberreiter, K., Kanig, G.: J. Colloid Sci. *7*, 569 (1952)
23. Couchman, P. R.: Polym. Eng. Sci. *21* (7), 377 (1981)
24. Kow, C., Morton, M., Fetters, L. J., Hadjichristidis, N.: Rubb. Chem. Tech. *55*, 245 (1982)
25. Fried, J. R.: in Developments in Polymer Characterisation-4, J. V. Dawkins, Ed., p. 39, Applied Science, London 1983
26. Horie, K., Hiura, H., Sawada, M., Mita, I.: J. Polym. Sci. A-1 *8*, 1357 (1970)
27. Macosko, C. W., Miller, D. R.: Macromolecules *9* (2), 199 (1976)
28. Miller, D. R., Macosko, C. W.: Macromolecules *9* (2), 206 (1976)
29. Prime, R. B.: in Thermal Characterization of Polymeric Materials, Turi, E. A., Ed., pp. 441, 480–482, Academic Press, N.Y. 1981
30. Prime, R. B.: Polym. Eng. Sci., *13* (5), 365 (1973)
31. Odian, G.: Principles of Polymerization, 2nd Ed., John Wiley & Sons, N.Y. 1981
32. Rosen, S. L.: Fundamental Principles of Polymeric Materials, 2nd Ed., John Wiley & Sons, N.Y. 1982
33. Kwant, P. W.: J. Polym. Sci.: Polym. Chem. Ed. *17*, 3397 (1979)

34. Horie, K., Mita, I., Kambe, H.: J. Polym. Sci. A-1, *6*, 2663 (1968)
35. Sundberg, D. C., James, D. R.: J. Polym. Sci.: Polym. Chem. Ed. *16*, 523 (1978)
36. Sourour, S., Kamal, M. R.: Thermochimica Acta *14*, 41 (1976)
37. Barton, J. M.: Polymer *21*, 603 (1980)

Editor: K. Dušek
Received August 19, 1985